

## Supplementary Information

### Fast and efficient electrical-thermal responses of functional nanoparticles decorated nanocarbon aerogels

Dong Xia,<sup>\*a</sup> Peng Huang,<sup>b</sup> Heng Li<sup>c</sup> and Noelia Rubio Carrero<sup>d</sup>

<sup>a</sup>School of Chemistry, University of Leeds, Leeds, LS2 9JT, UK

<sup>b</sup>School of Engineering and Physical Sciences, Heriot-Watt University, Edinburgh, EH14 4AS, UK

<sup>c</sup>Key Laboratory of Estuarine Ecological Security and Environmental Health, Tan Kah Kee College, Xiamen University, 363105, Zhangzhou, China

<sup>d</sup>Department of Chemistry, Imperial College London, SW7 2AZ, UK

\*Corresponding author: cmdx@leeds.ac.uk

#### Experimental section

**Materials:** Graphene oxide (GO) were purchased from William Blythe Limited. Carboxylic-acid-functionalised multi-walled carbon nanotube (oCNT), commercial boron nitride (BN) powder,  $\text{Al}(\text{NO}_3)_3 \cdot 9\text{H}_2\text{O}$  (98%),  $\text{Mg}(\text{NO}_3)_2 \cdot 6\text{H}_2\text{O}$  (99%), sucrose and polyvinyl alcohol (PVA) were obtained from Sigma-Aldrich. Sodium hydroxide (NaOH), sodium carbonate ( $\text{Na}_2\text{CO}_3$ ) and HPLC water were supplied by Fisher Scientific UK. All chemicals were used as received.

**Synthesis of MgAl-MMO precursors (MgAl-LDH):** A co-precipitation method was used to prepare different MgAl-LDH wet pastes. To produce MgAl-MMO/rGO aerogel (nominal loading of 50 wt%), the mixture (1.61 mL) of 0.5 M  $\text{Mg}(\text{NO}_3)_2 \cdot 6\text{H}_2\text{O}$  and 0.25 M  $\text{Al}(\text{NO}_3)_3 \cdot 9\text{H}_2\text{O}$  was added dropwise into an alkaline solution (5 mL) of 4.7 M NaOH and 1.2 M  $\text{Na}_2\text{CO}_3$ . The obtained white suspension was kept at 60 °C for 16 h, under magnetic stirring, to produce white precipitates. Subsequently, the white precipitates were washed with HPLC water to pH neutral. After washing, the white MgAl-LDH precipitates were kept in wet conditions for the following decoration onto nanocarbon aerogels. To produce MgAl-MMO/rCNT aerogel (nominal loading of 41 wt%), 1.12 mL liquid mixture of 0.5 M  $\text{Mg}(\text{NO}_3)_2 \cdot 6\text{H}_2\text{O}$  and 0.25 M  $\text{Al}(\text{NO}_3)_3 \cdot 9\text{H}_2\text{O}$  was used.

**Synthesis of MgAl-MMO decorated rGO aerogels and rCNT aerogels:** Nanocarbons (GO or oCNT powder, 75 mg) and organic additives (PVA and sucrose in a 1:1 weight ratio, 75 mg) were mixed in 10 mL HPLC water, sonicated to generate a uniform nanocarbon suspension. Into which, the pre-prepared wet MgAl-LDH paste was added to form a well-dispersed MgAl-LDH/Nanocarbon suspension using ultra-sonication. The resultant suspension (3.3 mL) was cast into a bespoke cylindrical mould (diameter 1.8 cm, height 1.6 cm) for unidirectional freezing in liquid nitrogen. Afterwards, the sample was freeze-dried (LABCONCO) overnight to obtain the MgAl-LDH/Nanocarbon aerogels. Finally, the aerogels were thermally reduced at 1000 °C, for 2 h, in  $\text{N}_2/\text{H}_2$  atmosphere (5%  $\text{H}_2$ ), using a tube furnace (Carbolite Gero Limited) to obtain the MgAl-MMO/rNanocarbon aerogels with an inorganic nanoparticle loading of 50 wt% in the MgAl-MMO/rGO aerogel and 41 wt% in the MgAl-MMO/rCNT aerogel.

**Synthesis of commercial BN decorated rGO aerogels and rCNT aerogels:** The decoration procedure of commercial BN onto nanocarbon aerogels was similar to the fabrication of MgAl-MMO/rNanocarbon aerogels. Specifically, 75 mg (or 52 mg for oCNT) BN powder was added into the GO suspension, followed by dispersion, freezing, freeze-drying and thermal reduction to produce the respective BN/rGO aerogel (nominal BN loading of 50 wt%) and BN/rCNT aerogel (nominal BN loading of 41 wt%).

**Joule-heating measurements:** Joule heating measurements of the prepared hybrid aerogels in this work were carried out in a custom-made setup. Before the measurements, all the aerogels were pre-conditioned at a Joule heating core temperature of 150 °C for 20 min to remove impurities (such as adsorbed water and gases), which is essential for the following Joule heating measurements (Fig. S2). After preconditioning, stepwise Joule heating was conducted by increasing the electrical current and held for 10 min at each step. The Joule heating temperature, voltage and current were recorded during the experiments (Fig. S3 and Fig. S4). The heating/cooling curves of the aerogel at a Joule heating energy of 2 W were recorded using a thermocouple (K grounded tip insulated probe with a thermocouple data logger, RS Components Ltd). For the electrical-thermal stability test, the hybrid aerogels were repeatedly heated and cooled for at least 10 times at a Joule heating energy of 2 W. Thermal conductivity was measured according to a previously reported radial temperature gradient fitting method.<sup>1</sup>

**Materials characterisation:** Powder X-ray diffraction (XRD) was performed on a Bruker D2 Phaser Diffractometer using Cu K<sub>α</sub> radiation. Scanning electron microscopic (SEM) analysis was conducted on a Nova NanoSEM 450 model with an accelerating voltage of 3 kV. Samples were fixed onto alumina stubs using conducting carbon tapes. Raman spectroscopic analysis was carried out using a Renishaw InVia Raman microscope with an excitation laser wavelength of 532 nm between 400 and 4000 cm<sup>-1</sup>. Infrared spectroscopic analysis (IR) was measured using a PerkinElmer Spectrum One IR Spectrometer, with the scanning range from 550 to 4000 cm<sup>-1</sup>. Thermal images were taken using a Fluke TiR1 thermal camera. The obtained data were analysed using the Fluke Connect software. Thermogravimetric analysis (TGA) was performed on a PerkinElmer Pyris One instrument in air atmosphere at a heating rate of 10 °C min<sup>-1</sup>, from ambient temperature to 850 °C. X-ray photoelectron spectroscopic analysis (XPS) was performed on a Thermo Scientific K-Alpha<sup>+</sup> XPS Spectrometer. High-resolution scans were collected at pass energy of 30 eV and a step size of 0.1 eV. The binding energies were referenced to the C1s peak of adventitious carbon at 284.8 eV.

## Results and discussion

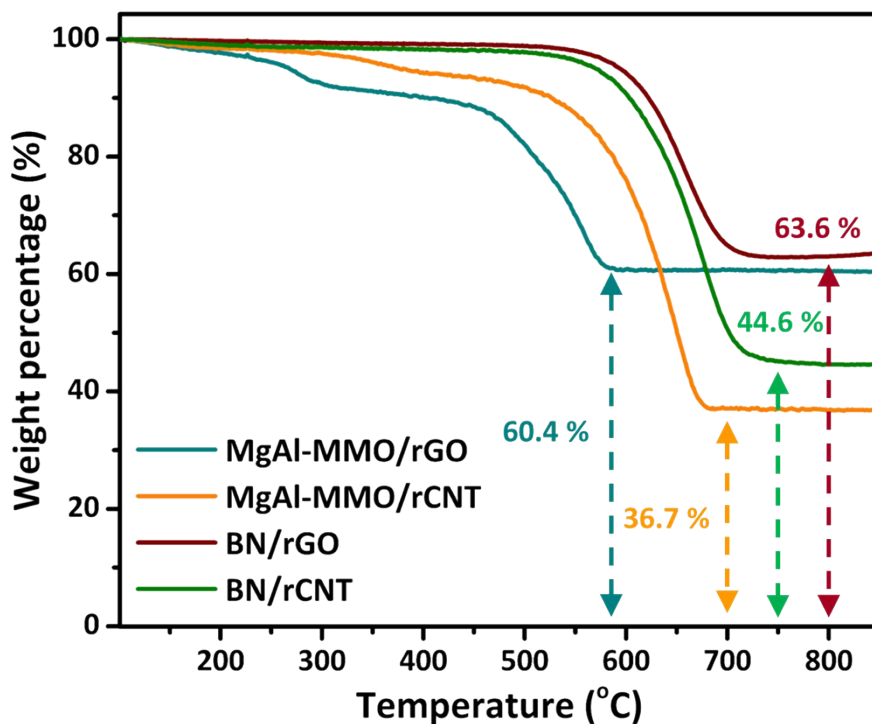


Fig. S1 TGA curves of different hybrid aerogels in air atmosphere.

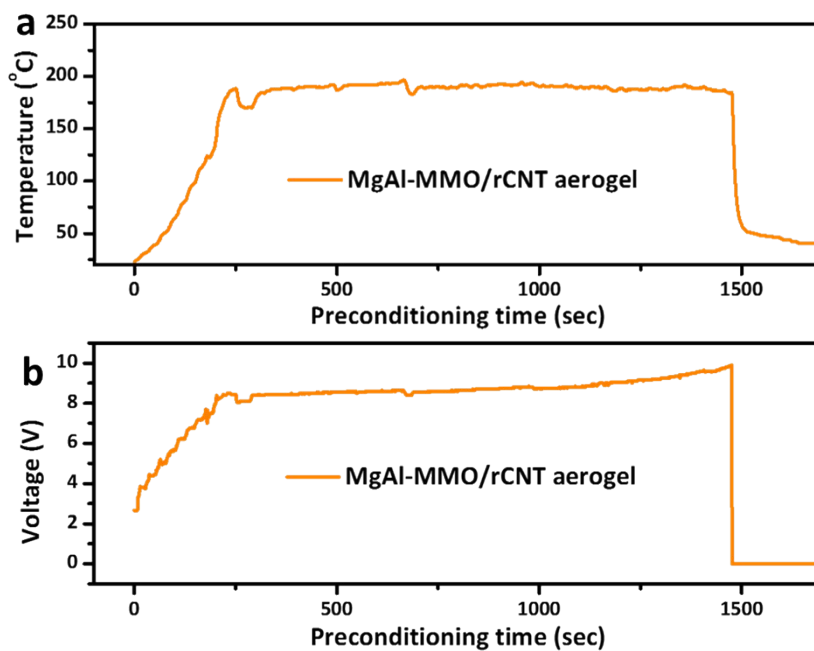


Fig. S2 Preconditioning Joule heating temperature (a) and voltage (b) of MgAl-MMO/rCNT aerogel.

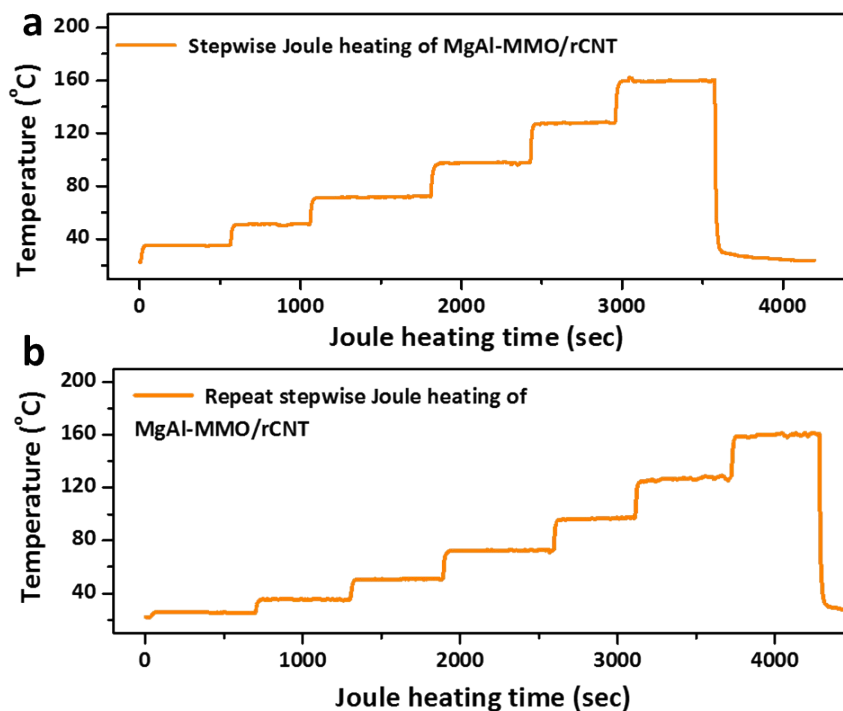


Fig. S3 Stepwise Joule heating temperature (a) and the repeat process (b) of MgAl-MMO/rCNT aerogel.

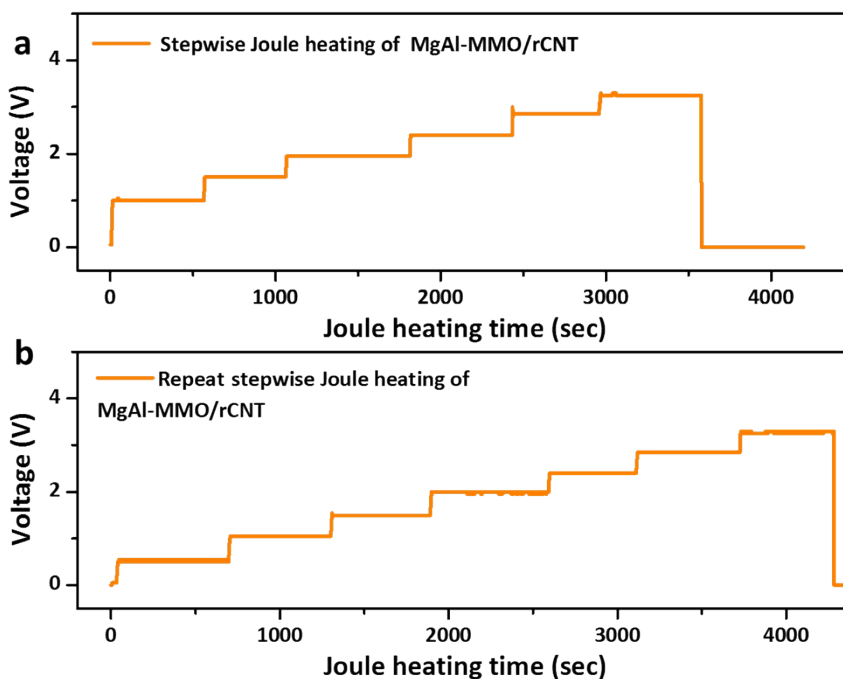


Fig. S4 Stepwise Joule heating voltage (a) and the repeat process (b) of MgAl-MMO/rCNT aerogel.



**Fig. S5** A simple compressibility test of the MgAl-MMO/rCNT aerogel under vial compression.

**Table S1.** The atomic percentage of elements in the hybrid aerogels

Aerogel	C1s (at %)	O1s (at %)	Mg1s (at %)	Al2p (at %)	B1s (at %)	N1s (at %)
MgAl-MMO/rGO	75.92	17.66	3.26	3.16	--	--
MgAl-MMO/rCNT	85.22	11.06	2.56	1.56	--	--
BN/rGO	81.48	4.31	--	--	8.52	5.69
BN/rCNT	80.11	7.33	--	--	8.12	4.44

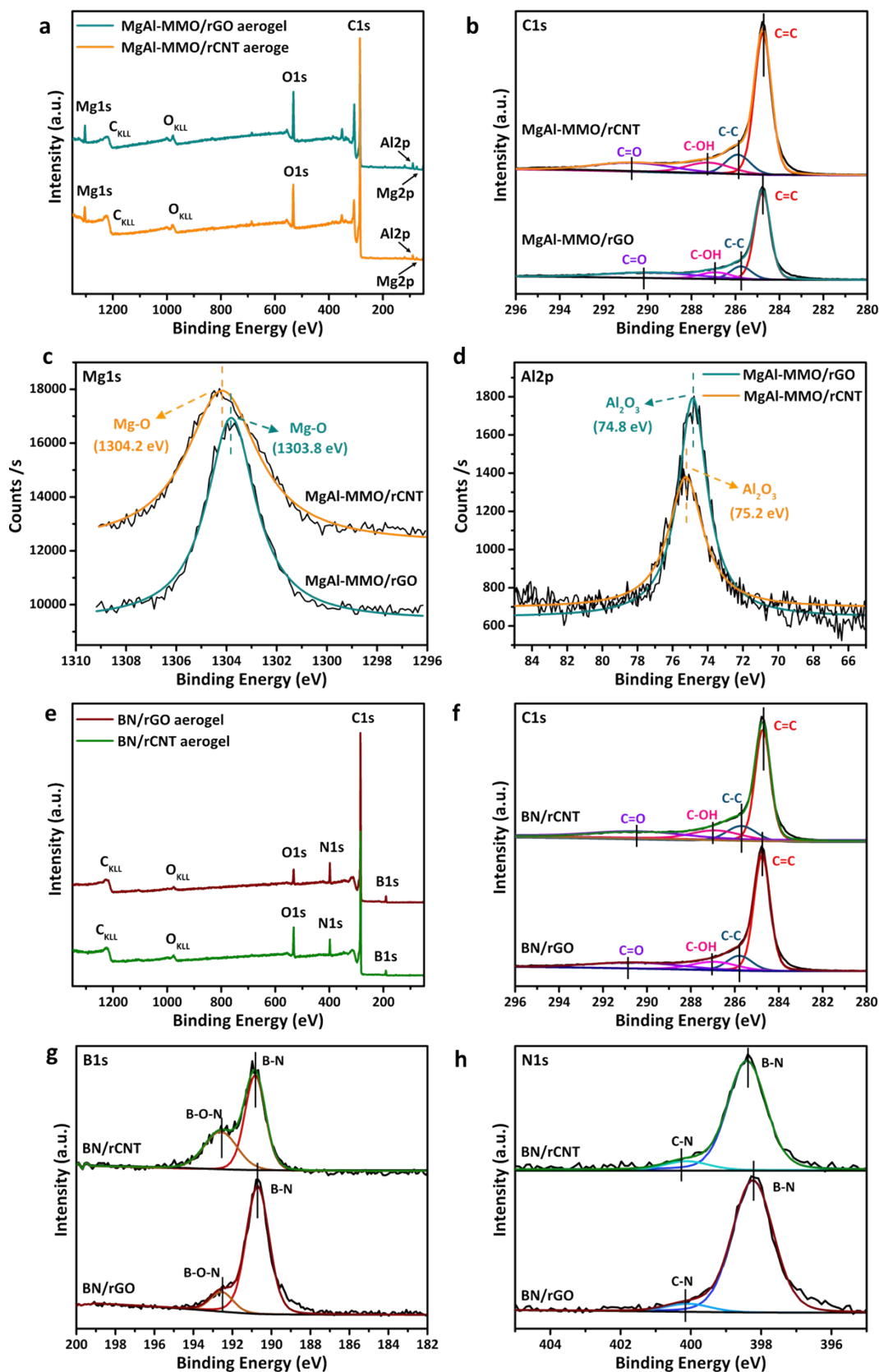


**Fig. S6** XPS spectra of MgAl-MMO/rGO aerogel and MgAl-MMO/rCNT aerogel. XPS full spectra (a). High-resolution XPS scan of C1s (b), Mg1s (c) and Al2p (d). XPS spectra of BN/rGO aerogel and BN/rCNT aerogel. XPS full spectra (e). High-resolution XPS scan of C1s (f), B1s (g) and N1s (h).

XPS analysis was conducted to elucidate the structural characteristics of the hybrid aerogels (Fig. S6). For the MgAl-MMO/rGO aerogel and MgAl-MMO/rCNT aerogel, only the elements of C, O, Mg and Al are observed in the hybrid aerogels (Fig. S6a), while the BN/rGO aerogel and BN/rCNT aerogel show the elements of C, O, B and N (Fig. S6e). The high-resolution C1s peaks of all hybrid aerogels exhibit typical nanocarbon compositions after high-temperature annealing, including C=C, C-C, C-OH and C=O groups, in line with reported studies (Fig. S6b and Fig. S6f).<sup>1</sup> Deconvolution of the high-resolution XPS Mg1s peak proves that Mg-O bonds are dominant, consistent with the XRD results (e.g. MgO and MgAl<sub>2</sub>O<sub>4</sub> are formed after thermal annealing, Fig S6c).<sup>2</sup> The high-resolution Al2p peak shows that the Al elements are in the form of aluminium oxides (Fig. S6d).<sup>3</sup> Detailed analysis of high-resolution B1s and N1s peaks demonstrate that the BN powders in both the BN/rCNT aerogels and BN/rGO aerogels have maintained the original -B-N- bonding structures (Fig. S6g and Fig. S6h),<sup>4</sup> owing to their ultra-high thermal stabilities. XPS results further confirm that the active substances are well exposed on the surface of the nanocarbons.

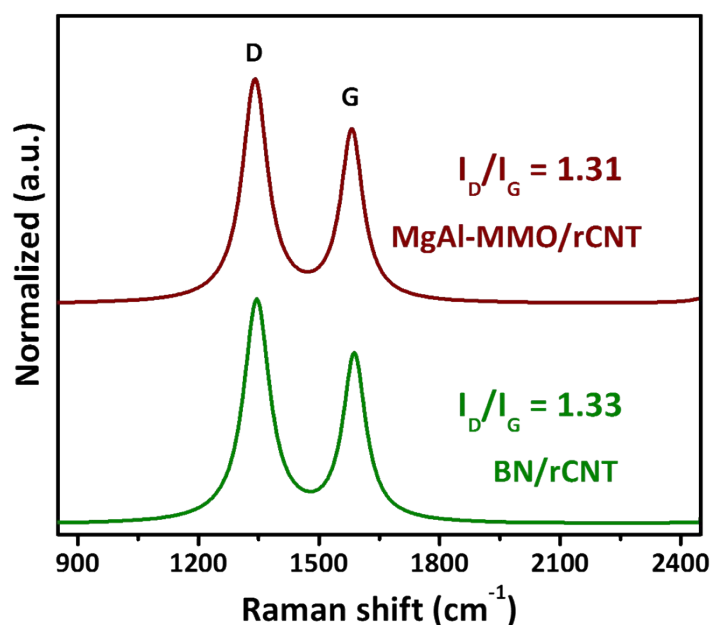
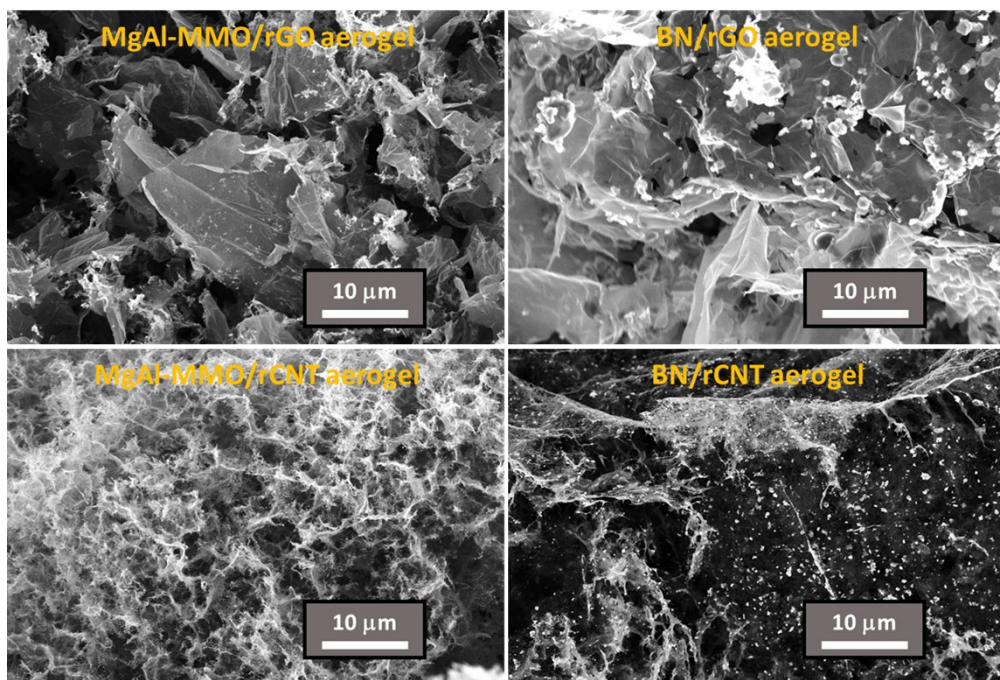
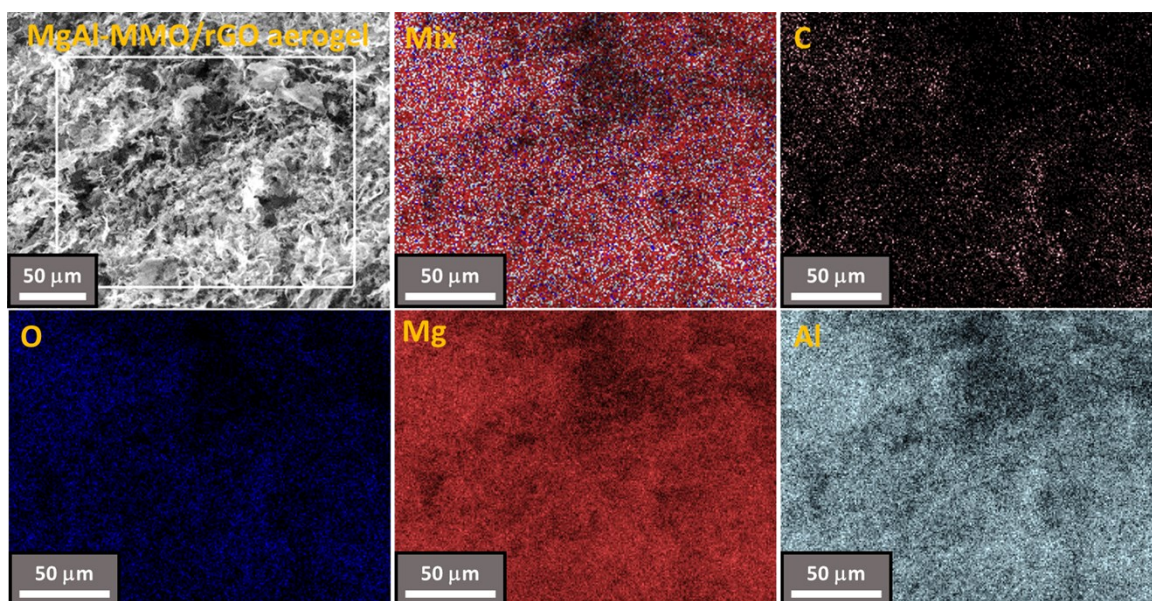


Fig. S7 Raman spectra of MgAl-MMO/rCNT aerogel and BN/rCNT aerogel.



**Fig. S8** Low-magnification SEM micrographs of the hybrid nanocarbon aerogels.



**Fig. S9** SEM micrograph and EDX mapping of MgAl-MMO/rGO aerogel.

**Table S2.** Parameters of the pure and functional nanoparticles decorated nanocarbon aerogels.

Samples	$\rho^a)$ (mg/cm <sup>3</sup> )	$\sigma^b)$ (S/m)	$\kappa^c)$ (W·m <sup>-1</sup> ·K <sup>-1</sup> )	T <sup>d)</sup> (°C)
rGO aerogel	5.5	11.4	0.143	123
MgAl-MMO/rGO aerogel	14.1	15.6	0.193	134
BN/rGO aerogel	12.9	9.8	0.165	125
rCNT aerogel	9.0	8.0	0.105	167
MgAl-MMO/rCNT aerogel	9.4	13.2	0.095	161
BN/rCNT aerogel	12.3	4.7	0.181	108

<sup>a)</sup> $\rho$  represents aerogel density; <sup>b)</sup> $\sigma$ , <sup>c)</sup> $\kappa$  and <sup>d)</sup>T represent electrical conductivity, thermal conductivity and aerogel core temperature, respectively. The heating power is 2W.

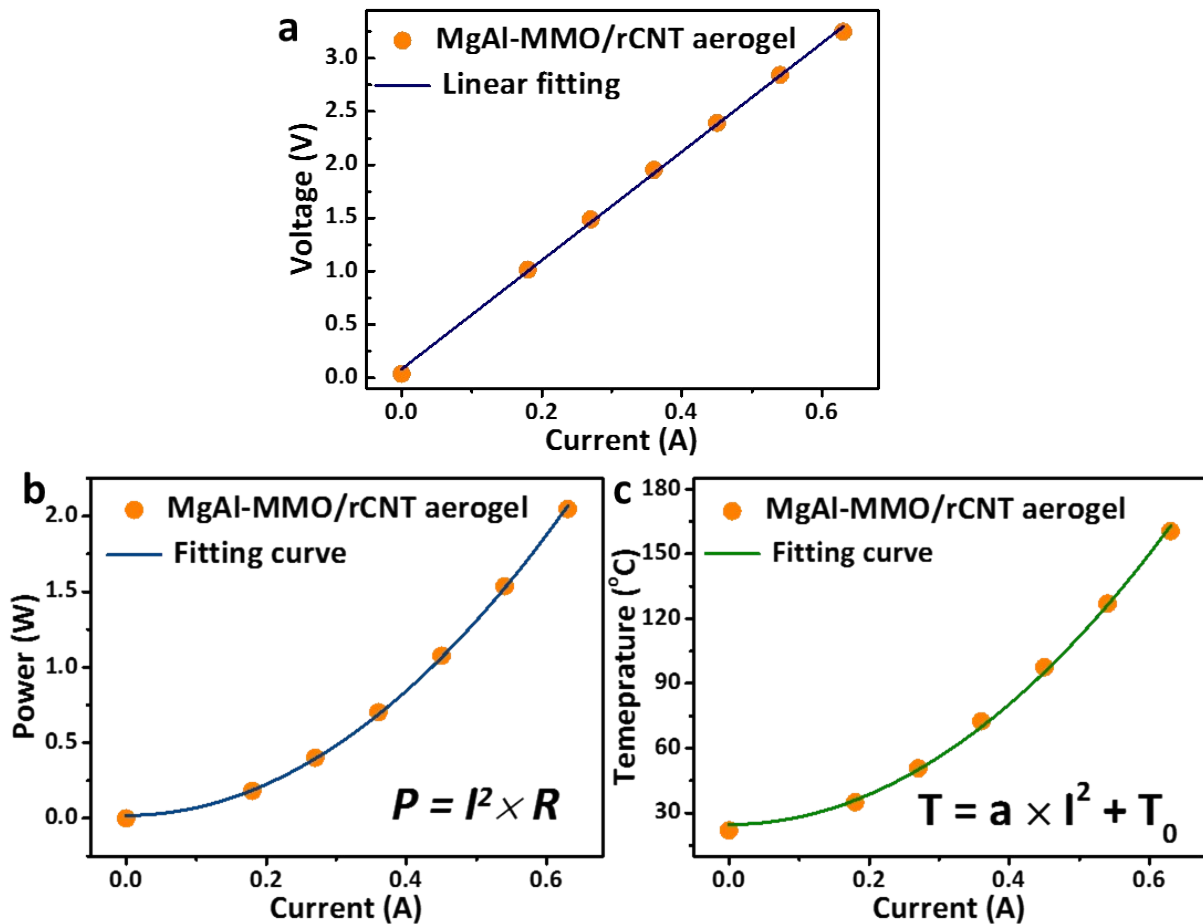


**Fig. S10** (a) I-U, I-P and I-T curves of MgAl-MMO/rCNT aerogel during Joule heating measurements.

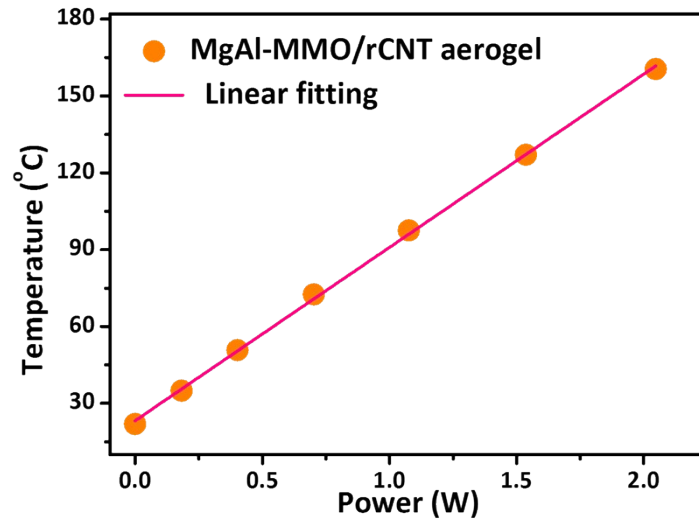


**Fig. S11** Relationship between Joule heating power input and the generated temperature of MgAl-MMO/rCNT aerogel.

The 3D variable range hopping (VRH) model is described as  $\sigma(T) = \sigma_0 \cdot T^{-1/2} \cdot \exp(-(T_0/T)^{1/4})$ ; here  $\sigma$  is the electrical conductivity ( $\text{S m}^{-1}$ ),  $\sigma_0$  is the electrical conductivity pre-factor,  $T_0$  is the temperature coefficient, and  $T$  is the Joule heating temperature.

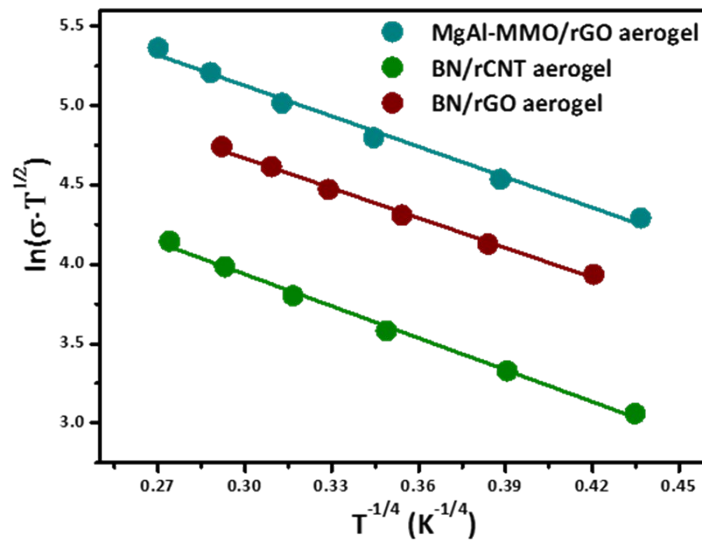


**Fig. S12** 3D VRH model fittings of different hybrid aerogels.

Importantly, all the prepared aerogels in this work, including MgAl-MMO/rGO, BN/rGO, MgAl-MMO/rCNT and BN/rCNT, exhibit a similar temperature-swing behaviour, crucial for nanoparticle regeneration via local resistive heating (Fig. S13-S16).

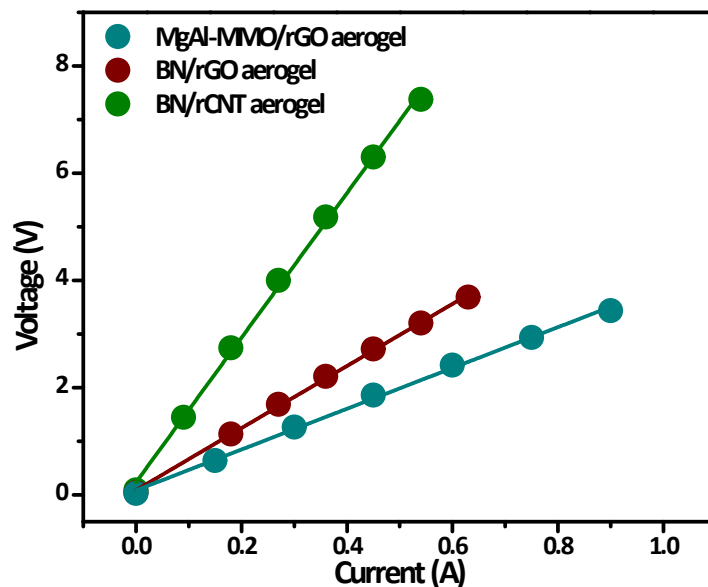


Fig. S13 Joule heating voltage versus current of different hybrid aerogels.

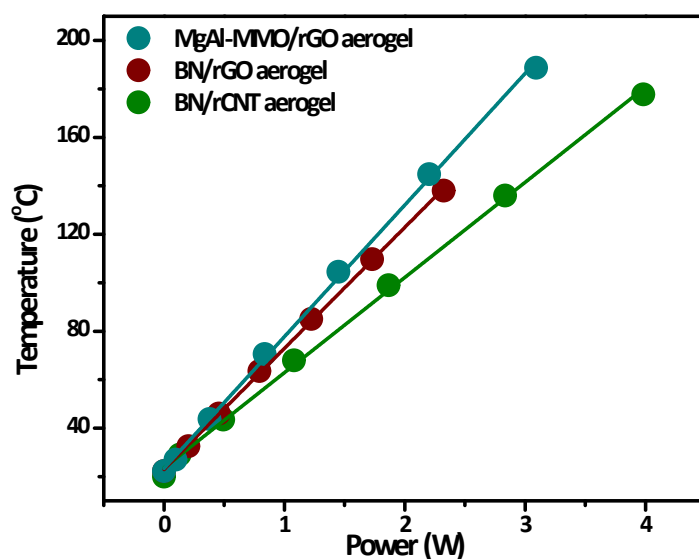


Fig. S14 Joule heating temperature versus power input of different hybrid aerogels.

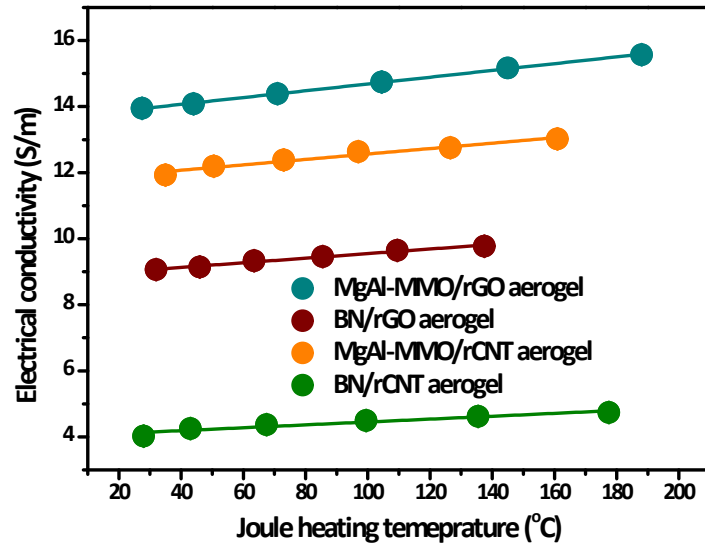


Fig. S15 Electrical conductivity versus Joule heating temperature of different hybrid aerogels.

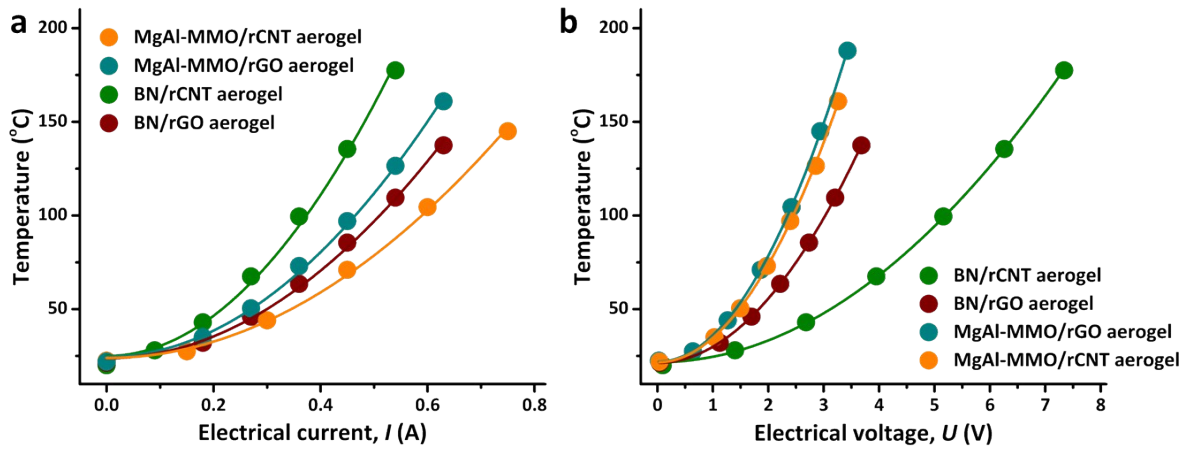
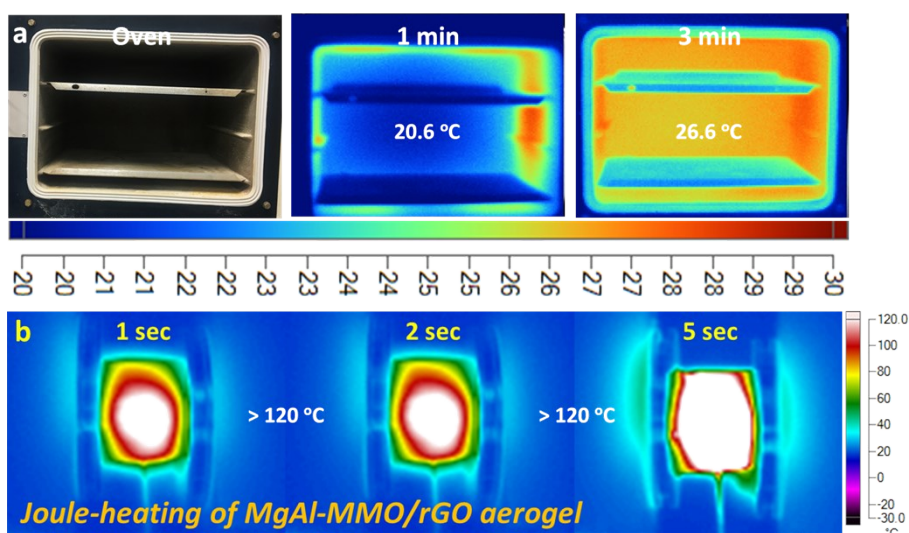


Fig. S16 Relationships between Joule heating temperature and electrical current/voltage of different hybrid aerogels



**Fig. S17** Thermal images of an oven via external heating (a) and MgAl-MMO/rGO aerogel via ultra-fast Joule heating (b).

Heating and cooling kinetics of the hybrid aerogels during the Joule heating experiments were analysed using the bi-exponential function, as described below:

$$T = A_1 e^{\frac{t}{\tau_1}} + A_2 e^{\frac{t}{\tau_2}} + T_0$$

Here,  $T$  (°C) is the measured Joule heating temperature at time  $t$ ,  $T_0$  represents the starting temperature (°C),  $\tau_1$  is the heating/cooling stage lifetime parameter (s),  $\tau_2$  is the equilibrium stage lifetime parameter (s), and  $A$  is the pre-exponential factor (°C). The Joule heating kinetics and natural cooling kinetics of all the hybrid aerogels can be well fitted using the bi-exponential function. The corresponding fitting parameters are listed in Table S3.

**Table S3.** Parameters for Joule heating and natural cooling of the hybrid aerogels, using the bi-exponential model fitting

Hybrid aerogel	Joule heating kinetics					Natural cooling kinetics				
	$\tau_1$ (s)	$\tau_2$ (s)	$A_1$	$A_2$	$T_0$	$\tau_1$ (s)	$\tau_2$ (s)	$A_1$	$A_2$	$T_0$
MgAl-MMO/rGO	-6.0	-303	-107	-9.3	136	-6.4	-181	102	11.5	25
BN/rGO	-7.5	-327	-107	-6.3	126	-8.4	-267	105	7.9	24
MgAl-MMO/rCNT	-7.1	-7.3	-143	0.23	163	-7.8	-219	140	7.1	23
BN/rCNT	-9.3	-458	-83	-7.8	110	-8.3	-275	79	8.7	24

## Reference

- 1 R. Menzel, S. Barg, M. Miranda, D.B. Anthony, S.M. Bawaked, M. Mokhtar, S.A. Al-Thabaiti, S.N. Basahel, E. Saiz and M.S. Shaffer, *Adv. Funct. Mater.*, 2015, **25**, 28-35.
- 2 R.K. Mishra, G.J. Choi, Y. Sohn, S.H. Lee and J.S. Gwag, *Chem. Commun.*, 2020, **56**, 2893-2896.
- 3 J. Kuljiraseth, A. Wangriya, J.M.C. Malones, W. Klysubun and S. Jitkarnka, *Appl. Catal. B Environ.*, 2019, **243**, 415-427.
- 4 Y. Cheng, J. Lin, T. Wu, H. Wang, S. Xie, Y. Pei, S. Yan and B. Zong, *Appl. Catal. B Environ.*, 2017, **204**, 475-485.
- 5 J. Xiong, L. Yang, Y. Chao, J. Pang, P. Wu, M. Zhang and H. Li, *Green Chem.*, 2016, **18**, 3040-3047.